Pharmacokinetics Research Laboratories[1]; Central Research Laboratories[2]; Toxicological Laboratories[3], Kissei Pharmaceutical Co., Ltd., Nagano, Japan

Species differences in the metabolism of ritobegron *in vitro* and assessment of potential interactions with transporters and cytochrome P450 enzymes

Y. Abe[1], E. Ota[1], H. Harada[1], H. Kanbe[2], Y. Kojima[2], T. Kanazawa[3], T. Endo[1], M. Murakami[1], M. Kobayashi[2]

Received July 27, 2014, accepted September 2, 2014

Yoshikazu Abe, Kissei Pharmaceutical Co., Ltd.,[1] 19-48 Yoshino, Matsumoto-City, Nagano-Pref. 399-8710, Japan

Pharmazie 70: 38–46 (2015) *doi: 10.1691/ph.2015.4733*

Ritobegron, a selective β_3-adrenoceptor agonist, is the prodrug of the active compound, KUC-7322. We investigated species differences in its metabolism *in vitro* and the potential for drug–drug interactions with ritobegron. In rat, dog, monkey, and human liver microsomes, ritobegron was not metabolized by cytochrome P450 enzymes (CYPs). KUC-7322 was the only metabolite observed. Hydrolysis of ritobegron to KUC-7322 was likely catalyzed by carboxylesterases in human liver microsomes. The maximum velocity of the reaction (V_{max})/Michaelis-Menten constant (K_m) for hydrolysis of ritobegron to KUC-7322 was much higher in rat serum than those in other species. There were also species differences in the conjugation of KUC-7322. Sulfate conjugates of ritobegron were detected in all species, whereas glucuronide and glutathione conjugates of KUC-7322 were only observed in rat liver subcellular fractions. Ritobegron and KUC-7322 did not affect the CYP-mediated metabolism of probe substrates in human liver microsomes and organic anion transporter 1 (OAT1)-, OAT2-, OAT3-, organic cation transporter 2 (OCT-2)-, OCT3-, or organic cation/carnitine transporter 1 (OCTN1)-mediated uptake of probe substrates in S2 cells. Ritobegron, but not KUC-7322, inhibited P-glycoprotein-mediated digoxin transport in Caco-2 cells. Significant uptake of KUC-7322 was observed in OAT3-expressing S2 cells. Therefore, CYP-mediated drug-drug interactions are not likely when ritobegron is administered with CYP substrates or inhibitors. Ritobegron may increase the plasma concentrations of P-glycoprotein substrates, such as digoxin, and the plasma concentration of KUC-7322 may increase when it is administered in combination with OAT inhibitors such as probenecid.

1. Introduction

Ritobegron (KUC-7483, the ethyl ester prodrug of KUC-7322) is a novel, selective β_3-adrenoreceptor (β_3-AR) agonist that may be useful for the treatment of overactive bladder (OAB). *In vitro* studies using CHO cells expressing human β-ARs revealed that the selectivity of ritobegron for β_3-AR was 301-fold and 32-fold higher than for β_1-AR and β_2-AR, respectively (Maruyama et al. 2012a). *In vivo* studies indicated that ritobegron induced a dose-dependent decrease in intravesical pressure without affecting heart rate in rats and cynomolgus monkeys (Maruyama et al. 2012b). A study using isolated human detrusor muscle showed

Table 1: Kinetic parameters for hydrolysis of ritobegron to KUC-7322 in liver S9 fractions from rat, dog, monkey, and human

	K_m (μM)	V_{max} (nmol/min/mg protein)	V_{max}/K_m (CL_{int}) (mL/min/mg protein)
Rat	309	626	2.02
Dog	25	68	2.76
Monkey	85	222	2.60
Human	212	959	4.53

Each value represents the mean of duplicates.
Ritobegron was incubated with liver S9 fractions from rat, dog, monkey, or human in 50 mM Tris-HCl buffer (pH 7.4, containing 0.154 M KCl) for 5 min at 37 °C.
Ritobegron concentrations: 5, 10, 20, 50, 100, 200, 500, and 1,000 μM.
Liver S9 protein content: rat (0.0520 mg/mL), dog (0.0491 mg/mL), monkey (0.0483 mg/mL), and human (0.0250 mg/mL).
K_m: Michaelis-Menten constant, V_{max}: maximum velocity of reaction, CL_{int}: intrinsic clearance

Abbreviations: AR, adrenoceptor; BNPP, bis (*p*-nitrophenyl) phosphate; CYP, cytochrome P450 enzymes; DDI, drug-drug interaction; GSH, glutathione (γ-glutamyl-L-cysteinylglycine); K_m, Michaelis-Menten constant; $NADP^+$, β-nicotineamide adenine dinucleotide phosphate; oxidized form; NADPH, β-nicotineamide adenine dinucleotide phosphate; reduced form; OAB, overactive bladder; P_{app}, apparent permeability; PAPS, adenosine 3'-phosphate 5'-phosphosulfate; P-gp, P-glycoprotein; PMSF, phenylmethanesulfonyl fluoride; SPE, solid-phase extraction; UDPGA, uridine 5'-diphosphoglucuronic acid; V_{max}, maximum velocity of the reaction Ritobegron: (-)-ethyl 2-[4-(2-{[(1*S*,2*R*)-2-hydroxy-2-(4-hydroxyphenyl)-1-methylethyl]amino}ethyl)-2,5-dimethylphenyloxy] acetate monohydrochloride; KUC-7322, 2-[4-(2-{[(1*S*,2*R*)-2-hydroxy-2-(4-hydroxyphenyl)-1-methylethyl]amino}ethyl)-2,5-dimethylphenyloxy]acetic acid; UL092, 2-[2,3-Dichloro-4-(2-{[(1*S*,2*R*)-2-hydroxy-2-(4-hydroxyphenyl)-1-methylethyl]amino}ethyl) phenoxy]-acetic acid; KUR-1243, 1-(2-{[(2*S*)-2-({(2*R*)-2-hydroxy-2-[4-hydroxy-3-(2-hydroxyethyl)phenyl]ethyl}amino)-1,2,3,4- tetrahydronaphthalen-7-yl] oxy}acetyl)piperidine.

Table 2: Kinetic parameters for hydrolysis of ritobegron to KUC-7322 in serum from rat, dog monkey, and human

	Low affinity			High affinity		
	K_m	V_{max}	V_{max}/K_m	K_m	V_{max}	V_{max}/K_m
	(μM)	(nmol/min/mL)	(min^{-1})	(μM)	(nmol/min/mL)	(min^{-1})
Rat	189	3.02×10^4	159	11.9	5.23×10^3	441
Dog	128	146	1.14	–	–	–
Monkey	327	82.2	0.252	16.4	10.5	0.640
Human	126	112	0.890	4.64×10^{-4}	2.92	6.28×10^3

Each value represents the mean of duplicates.
Ritobegron was incubated with serum from rat, dog, monkey, or human in 50 mM Tris-HCl buffer (pH 7.4, containing 0.154 M KCl) for 5 min at 37 °C.
Ritobegron concentrations: 5, 10, 20, 50, 100, 200, 500, and 1,000 μM.
Added serum volume: rat (0.5 μL/mL), dog (50 μL/mL), monkey (100 μL/mL) and human (50 μL/mL)
K_m: Michaelis-Menten constant, V_{max}: maximum velocity of reaction

that KUC-7322, the active form of ritobegron, relaxed detrusor preparations and decreased carbachol-induced bladder contraction in a concentration-dependent manner (Igawa et al. 2012). Based on these data, it was hypothesized that ritobegron may be useful for treatment of OAB.

We previously reported the pharmacokinetic profiles of ritobegron and KUC-7322 after oral administration in rats (Abe et al. 2014). Ethyl esterification of KUC-7322 to form ritobegron enhanced both the area under the concentration-time curve ($AUC_{0\text{-}t}$) and maximum concentration of the drug (C_{max}) by 10-fold, and a substantial first-pass effect was observed. Following oral administration of [^{14}C]ritobegron, radioactivity distributed rapidly throughout the whole body. Radioactivity in tissues, excluding those tissues involved in administration, absorption, metabolism, and excretion, was lower than that in plasma. In metabolic analysis, it was observed that ritobegron was rapidly metabolized to KUC-7322, which was then metabolized primarily to the glucuronide conjugate. The objective of the present study was to investigate species differences in the metabolism of ritobegron *in vitro* and the inhibition of influx/efflux transporters and cytochrome P450 (CYP)-mediated metabolism of probe substrates. From these investigations, we studied the potential for drug-drug interactions (DDI) with ritobegron.

2. Investigations and results

2.1. In vitro species differences in CYP metabolism

When [^{14}C]ritobegron was incubated in the absence of liver microsomes, little KUC-7322 was found in the reaction mixture (5.3% of total radioactivity). In the presence of liver microsomes, KUC-7322 was formed in microsomes from all species irrespective of the presence of NADPH. Moreover, [^{14}C]ritobegron was almost completely hydrolyzed to KUC-7322 (more than 99% in all cases). No metabolites other than KUC-7322 were found in any of the incubations.

2.2. In vitro species differences in the hydrolysis of ritobegron in liver S9 fractions

Kinetic parameters were calculated from Eadie-Hofstee plots for the hydrolysis of ritobegron to KUC-7322. The kinetic parameters were determined in hepatic S9 fractions from rat, dog, monkey, and human are summarized in Table 1 The Michaelis-Menten constants (K_m) had the rank order: rat > human > monkey > dog. The rank order of the maximum velocity of the reaction (V_{max}) was human > rat > monkey > dog. The V_{max}/K_m (expressed as intrinsic clearance) showed the rank order: human > dog > monkey > rat. The V_{max}/K_m in the human liver S9 fraction was approximately 2.2-, 1.6-, and 1.7-fold greater than the V_{max}/K_m values from rat, dog, and monkey, respectively.

Table 3: Comparison of [^{14}C]KUC-7322 glucuronide and sulfate conjugate formation activities in liver microsomes or S9 fractions from rat, dog, monkey, or human

	Conjugation activity (pmol/min/mg protein)	
Species	Glucuronide conjugation [1)]	Sulfate conjugation [2)]
Rats	61.09	11.58
Dog	ND	1.23
Monkey	ND	2.07
Humans	ND	1.62

Each value represents the mean of duplicates.
ND: Not detected, any peak of conjugates of KUC-7322 was not detected on the chromatogram of incubations.
1) For formation of glucuronide conjugates of KUC-7322, liver microsomes (1 mg protein/mL) were incubated at 37 °C for 120 min with 50 μM [^{14}C]KUC-7322 in 100 mM Tris-HCl buffer (pH 7.4) containing 5 mM $MgCl_2$, 0.5 mg/mg Brij 58, and 3 mM uridine 5'-diphosphoglucuronic acid (UDPGA).
2) For formation of sulfate conjugate of KUC-7322, liver S9 fractions (3 mg protein/mL) were incubated at 37 °C for 120 min with 50 μM [^{14}C]KUC-7322 in 100 mM phosphate buffer (pH 7.4) containing 5 mM $MgCl_2$, and 1 mM adenosine 3'-phosphate 5'-phosphosulfate (PAPS).

2.3. In vitro species differences in hydrolysis of ritobegron in serum

Eadie-Hofstee plots for hydrolysis of ritobegron to KUC-7322 in serum from rat, dog, monkey, and human are shown in Fig. 1. Kinetic parameters calculated from an Eadie-Hofstee plot or a two-enzyme Michaelis-Menten model for KUC-7322 formation are summarized in Table 2 The K_m or low K_m (for the two-enzyme model) showed the rank order: monkey > rat > dog > human. The rank order of V_{max} (for the single enzyme or the low K_m enzyme in the two-enzyme model) was rat > > dog > human > monkey. The V_{max}/K_m had the rank order: rat > > dog > human > monkey.

2.4. In vitro species differences in conjugate metabolite formation

The formation of glucuronide and sulfate conjugates in rat, dog, monkey, and human liver microsomes or S9 fractions is summarized in Table 3. The glucuronide conjugate was detected in rat liver microsomes, but not in dog, monkey, and human liver microsomes. The sulfate conjugate was detected in liver S9 fractions from all species. Formation rates of the sulfate conjugate in dog, monkey, and human liver S9 fractions were 11%, 18%, and 14% of the rate in rat liver S9 fraction.

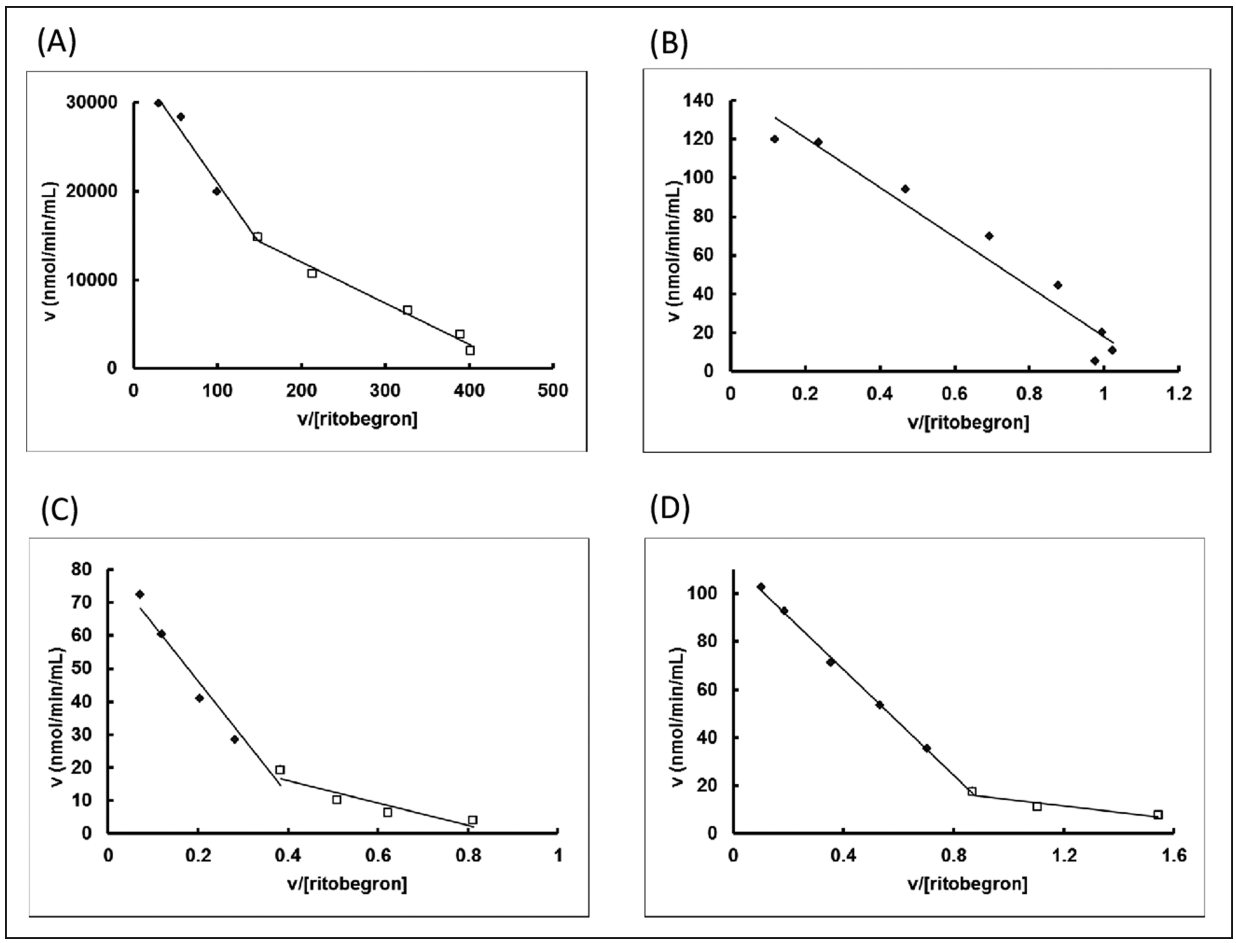

Fig. 1: Eadie-Hofstee plots for metabolism of ritobegron to KUC-7322 in serum from rat (A), dog (B), monkey (C), and human (D). Each point represents the mean of duplicates. Monkey serum-1000 μM shows the value of single assay. Ritobegron concentrations: 1000, 500, 200, 100, 50, 20, 10, and 5 μM. Added serum volume: rat (0.5 μL/mL), dog (50 μL/mL), monkey (100 μL/mL), human (50 μL/mL). Reaction time: 5 min.

Table 4: Effects of esterase inhibitors on hydrolysis of ritobegron in human liver microsomes

Esterase inhibitor	Inhibition (%)		
	10 μM	100 μM	1000 μM
PMSF	85.5	88.2	95.4
Eserine	ND	16.9	46.6
BNPP	87.5	90.4	89.5

Each value represents the mean of duplicates.
ND: Inhibition (%) was not calculated, because KUC-7322 concentration was below the lower limit of quantification.
PMSF: phenylmethanesulfonyl fluoride, BNPP: bis (*p*-nitrophenyl) phosphate,

The glutathione (GSH) conjugate was formed only in rat liver S9 fractions when adenosine 3'-phosphate 5'-phosphosulfate (PAPS) and GSH were added (4.5 pmol/min/mg protein). No GSH conjugate formation was observed in S9 fractions from any other species under any reaction conditions tested. In rats, the conjugate metabolites formed *in vitro* were the same as the metabolites determined *in vivo* (Abe et al. 2014).

2.5. Effects of esterase inhibitors on hydrolysis of ritobegron in human liver microsomes

Effects of esterase inhibitors on hydrolysis of ritobegron to KUC-7322 in human liver microsomes are summarized in Table 4. The hydrolysis of ritobegron was strongly inhibited by phenylmethanesulfonyl fluoride (PMSF), a serine protease inhibitor (James 1978; Kraut et al. 2000), and bis (*p*-nitrophenyl) phosphate (BNPP), a carboxylesterase inhibitor (White et al. 1987; Simeon et al. 1988). They inhibited KUC-7322 formation activity 85.5% and 87.5% from control, respectively, at a concentration of 10 μM. Eserine, a cholinesterase inhibitor (Simeon et al. 1988), did not inhibit the hydrolysis of ritobegron at 10 μM, but inhibited hydrolysis by 16.9% and 46.6% from control at concentrations of 100 and 1000 μM, respectively.

2.6. Effects of ritobegron and KUC-7322 on metabolism of CYP substrates in human liver microsomes

Effects of ritobegron and KUC-7322 on the metabolism of substrates of CYP1A2, 2A6, 2C9, 2C19, 2D6, 2E1, and 3A4 (7-ethoxyresorufin, coumarin, tolbutamide, *S*-mephenytoin, dextromethorphan, chlorzoxazone, and nifedipine, respectively) are summarized in Table 5. No significant inhibition of the metabolism of any probe substrates was observed when ritobegron and KUC-7322 were added at a concentration of 300 μM.

2.7. Effects of KUC-7322 on OAT-, OCT-, and OCTN-mediated substrate transport

The inhibitory effects of KUC-7322 on the uptake of radiolabeled probe substrates were assessed using S2 cells expressing organic anion transporter 1 (OAT1), OAT2, OAT3, organic cation transporter 2 (OCT2), OCT3, and organic cation/carnitine transporter 1 (OCTN1). The effects on uptake (expressed as percent of control uptake) of 30 μM KUC-7322 are summarized

Table 5: Effects of ritobegron and KUC-7322 on metabolism of cytochrome P450 (CYP) probe substrates

CYP isoform	Probe substrate[1)]	Residual CYP activity (%)[2)]			
		Ritobegron		KUC-7322	
		100 μM	300 μM	100 μM	300 μM
CYP1A2	7-Ethoxyresorufin	94.9	91.6	102.1	93.4
CYP2A6	Coumarin	96.3	104.7	98.0	101.0
CYP2C9	Tolbutamide	78.9	91.7	92.6	96.0
CYP2C19	*S*-Mephenytoin	89.1	111.0	117.2	104.4
CYP2D6	Dextromethorphan	96.9	106.9	104.6	104.2
CYP2E1	Chlorzoxazone	92.9	104.0	120.9	110.1
CYP3A4	Nifedipine	98.1	104.5	96.5	82.4

Each value represents the mean of triplicates.
Human liver microsomes were incubated with CYP probe substrates in 0.1 M potassium phosphate buffer (pH 7.4), 5 mM $MgCl_2$, 0.1 mM EDTA, 1 mM NADPH.
1) Probe substrates, 7-ethoxyresorufin, coumarin, tolbutamide, *S*-mephenytoin, dextromethorphan, chlorzoxazone, and nifedipine, were incubated at concentrations of 5, 5, 150, 50, 10, 50, and 10 μM, respectively. Human liver microsomes concentrations were 0.2, 0.05, 0.2, 1.0, 0.5, 0.1, and 0.1 mg protein/mL, respectively.
2) Metabolites of probe substrates, CYP1A2 – resorufin, 2A6 – 7-hydroxycoumarin, 2C9 – hydroxytolbutamide, 2C19 – 4'-hydroxymephenytoin, 2D6 – dextrorphan, 2E1 – 6-hydroxychlorzoxazone and 3A4 – oxidized nifedipine, were determined to calculate residual CYP activities.

Table 6: Effects of KUC-7322 on the uptake of probe substrates by OAT1, OAT2, OAT3, OCT2, OCT3, and OCTN1 expressed in S2 cells

Transporter	Probe substrate [1)]	Percentage of control uptake (%)		
		Unlabeled probe substrate	KUC-7322	Reference inhibitor [2)]
OAT1	[^{14}C]PAH	4.4	100.9	23.0
OAT2	[^{3}H]PGF2α	8.9	89.1	34.1
OAT3	[^{3}H]Estrone sulfate	23.2	79.4	31.2
OCT2	[^{14}C]TEA	51.2	103.5	64.1
OCT3	[^{3}H]Histamine	25.6	88.2	54.9
OCTN1	[^{14}C]TEA	29.2	98.6	31.9

Each value represents the mean of triplicates.
Reaction periods: OAT1, OAT3 for 2 min, OAT2 for 0.5 min, OCT2 and OCTN1 for 5 min, OCT3 for 1 min.
1) Substrate concentration: [^{14}C]PAH, [^{14}C]TEA, [^{3}H]histamine at 5 μM, [^{3}H]PGF2α, [^{3}H]estrone sulfate at 0.05 μM.
2) Reference inhibitor: probenecid for OAT1 and OAT3, benzbromarone for OAT2, imipramine for OCT2 and OCT3, and quinidine for OCTN1.
OAT: organic anion transporter, OCT: organic cation transporter, OCTN: organic cation/carnitine transporter, PAH: *p*-aminohippuric acid, PGF2α: prostaglandin F2α, TEA: tetraethylammonium.

in Table 6. OAT1-mediated [^{14}C]*P*-aminohippuric acid (PAH), OCT2-mediated [^{14}C]tetraethylammonium bromide (TEA), and OCTN-mediated [^{14}C]TEA uptake were not inhibited by KUC-7322. OAT2-mediated [^{3}H]prostaglandin F2α (PGF2α) and OCT3-mediated [^{3}H]histamine uptake were slightly inhibited by KUC-7322 (89.1% and 88.2% of control uptake, respectively). OAT3-mediated [^{3}H]estrone sulfate uptake was weekly inhibited by KUC-7322 (79.4% of control uptake).

2.8. Effects of ritobegron and KUC-7322 on P-glycoprotein (P-gp) mediated digoxin transport

The effects of ritobegron and KUC-7322 on P-gp-mediated digoxin transport were assessed by determining the efflux ratio (ER) of [^{3}H]digoxin across Caco-2 cell monolayers. The P_{app} (apparent permeability) and ER of [^{3}H]digoxin in the presence or absence (control) of ritobegron and KUC-7322 are summarized in Table 7. The ER of [^{3}H]digoxin was 3.1 in the control cells, and decreased to 1.5 by 100 μM of ritobegron but was not significantly affected by 100 μM KUC-7322. The IC_{50} value for the effects of ritobegron on P-gp-mediated digoxin transport was 58.2 μM (Fig. 2).

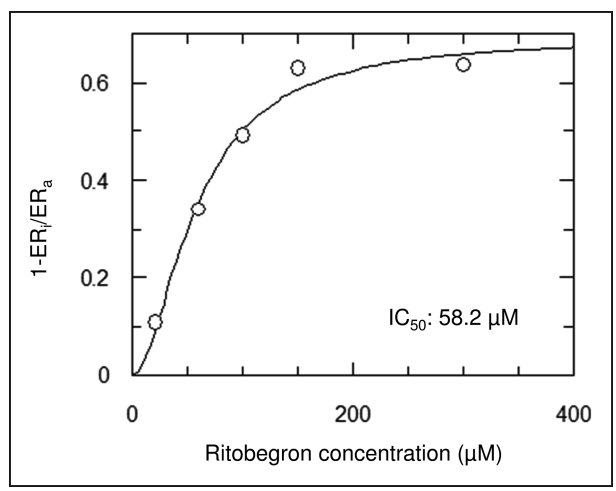

Fig. 2: Concentration-dependent inhibition by ritobegron of [3H]digoxin efflux across Caco-2 cell monolayers. Each point represents the mean of three determinations. Concentration of [3H]digoxin was 1 μM. ERi/ERa: Efflux ratio in the presence of inhibitor relative to efflux ratio in the absence of the inhibitor.

2.9. Uptake of KUC-7322 by OAT3

Time dependent uptake of [^{14}C]KUC-7322 in S2 cells expressing OAT3 is shown in Fig. 3. Uptake of [^{14}C]KUC-7322 increased almost linearly up to 5 min. Uptake activity was 1.8-, 2.5-, 2.8-, and 3.6-fold greater than in mock-transfected cells after incubation for 0.5, 1, 2, and 5 min, respectively. Significant uptake of [^{14}C]KUC-7322 was observed in OAT3 expressed S2 cells compared to mock-transfected cells. Apparent K_m and

Table 7: Effects of ritobegron and KUC-7322 on [^{3}H]digoxin permeability across Caco-2 cell monolayers

Group	P_{app} ($\times 10^{-6}$ cm/s)		ER
	$P_{A/B}$	$P_{B/A}$	($P_{B/A}/P_{A/B}$)
Control ([^{3}H]digoxin)	0.937 ± 0.059	2.949 ± 0.246	3.1
+ 100 μmol/L Ritobegron	1.799 ± 0.164	2.739 ± 0.194	1.5
+ 100 μmol/L KUC-7322	0.948 ± 0.141	2.857 ± 0.180	3.0
+ 100 μmol/L Verapamil *	2.266 ± 0.085	2.457 ± 0.154	1.1
^{3}H-Mannitol **	1.571 ± 0.147	1.323 ± 0.032	0.8

Values are the mean ± standard deviation of three determinations.
Concentrations of [^{3}H]digoxin and [^{3}H]Mannitol were 1 μmol/L.
P_{app}: apparent permeability, $P_{A/B}$: apparent permeability from apical to basal side, $P_{B/A}$: apparent permeability from basal to apical side, ER: efflux ratio
*: Positive control inhibitor
**: Paracellular marker

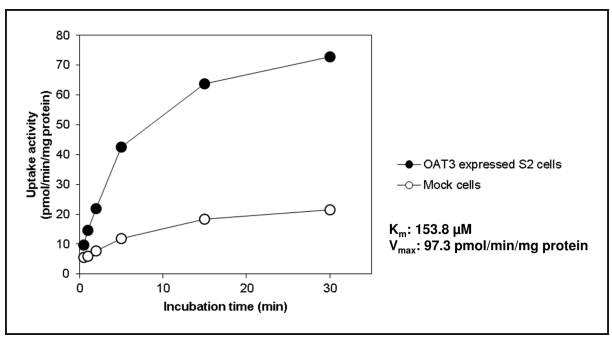

Fig. 3: Time-dependent [14C]KUC-7322 uptake by OAT3 expressed in S2 cells. Each point represents the mean of three determinations. [14C]KUC-7322 concentration: 10 μM.

V_{max} for KUC-7322 were calculated to be 153.8 μM and 97.3 pmol/min/mg protein, respectively.

3. Discussion

In this study, we investigated the species differences in the *in vitro* metabolism of ritobegron and potential for drug–drug interactions (DDI) with ritobegron. Ritobegron was hydrolyzed to KUC-7322 in liver microsomes from rat, dog, monkey, and human. Other metabolites were not detected. Hydrolysis of ritobegron was independent of NADPH. Both ritobegron and KUC-7322 were not metabolized by CYP enzymes in any of the species tested and there were no species differences in CYP metabolism of ritobegron.

The V_{max}/K_m for hydrolysis of ritobegron to KUC-7322 in human liver S9 fraction was 2.2-, 1.6-, and 1.7- fold greater than rat, dog, and monkey, respectively. Thus, there were small species differences in KUC-7322 formation in the liver. The K_m and V_{max} for hydrolysis of ritobegron to KUC-7322 in dog serum were determined from an Eadie-Hofstee plot. However, in rat, monkey, and human serum, the kinetic parameters were determined by fitting velocity *versus* substrate concentration curves using nonlinear least squares regression to a two-enzyme Michaelis-Menten model, because their Eadie-Hofstee plots were nonlinear. Therefore, it was demonstrated that multiple enzymes are involved in hydrolysis of ritobegron in rat, monkey, and human serum.

The $V_{max}/K_{m,}$ which indicates intrinsic clearance, was much larger for rat serum than for other species. Since hydrolysis of ritobegron in human liver microsomes was inhibited by PMSF and BNPP, it is likely that ritobegron is hydrolyzed by carboxylesterases (CESs: EC.3.1.1.1) in human liver. According to the current classification of esterases (Aldridge 1993), CES, a serine superfamily of esterases, falls into the B-esterase group. The CES is further classified into five major groups, based on homology of the amino acid sequences, and the majority of CESs belongs to the CES1 or CES2 (Hosokawa et al. 2007). CES1 is widely distributed in many tissues but is found at very low levels in the intestine. CES2 is widely distributed in the intestine, liver, and kidney (Satoh et al. 2002; Xu et al. 2002).

CES1 preferentially catalyzes hydrolysis of compounds esterified with a small alcohol group and a large acyl group. In contrast, CES2 hydrolyzes compounds with a relatively small acyl group and large alcohol group (Satoh et al. 2002; Imai et al. 2006). It is likely that CES1 is involved in hydrolysis of ritobegron in human liver and intestine, because ritobegron is esterified with small alcohol group, but this was not confirmed in this study.

In humans, CESs are primarily involved in drug hydrolysis in the liver, intestine, and other tissues, while cholinesterases and arylesterases are involved in drug hydrolysis in plasma (Williams 1985). There is a soluble CES in rodent plasma but not monkey and human plasma (Li et al. 2005). Thus, species differences in CESs might be reflected in hydrolysis of ritobegron to KUC-7322 in serum. It has been reported that hydrolysis of CPT-11 was mainly catalyzed by CES2 in human liver (Humerickhouse et al. 2000; Xu et al. 2002), whereas butyrylcholinesterase was involved in the hydrolysis in plasma (Morton et al. 1999). Therefore, it is possible that hydrolysis of ritobegron is also catalyzed by cholinesterases in serum.

The formation of the glucuronide and sulfate conjugates of KUC-7322 was observed in rat liver microsomes and S9 fractions, respectively. These results were consistent with a previous study in rats, in which KUC-7322 and its glucuronide, sulfate, and GSH conjugates were detected in plasma, bile, urine, and feces after oral administration of ritobegron (Abe 2014). In dog, monkey, and human liver microsomes and S9 fractions, little of the glucuronide and GSH conjugates were formed and the sulfate conjugate in these species was less than in rat liver S9 fractions. Therefore, it is likely that KUC-7322 is metabolized *in vivo* only to the sulfate conjugate in dogs, monkeys, and humans. The GSH conjugate of KUC-7322 was formed only in rat liver S9 fractions in the presence of both PAPS and GSH. Therefore, PAPS may be necessary to form GSH conjugate, and it is formed through a sulfate conjugate in rat liver S9 fractions.

The metabolic pathway determined from these results is shown in Fig. 4. Sulfate conjugation is generally considered the final step in the biotransformation and detoxification pathway of xenobiotics. Sulfate conjugates are more water-soluble and more easily excreted into the urine. However, sulfate conjugation leads to bioactivation of certain types of compounds including benzylic, allylic alcohols, and aromatic hydroxylamines. Sulfate conjugates of these compounds undergo loss of HSO_4^-,

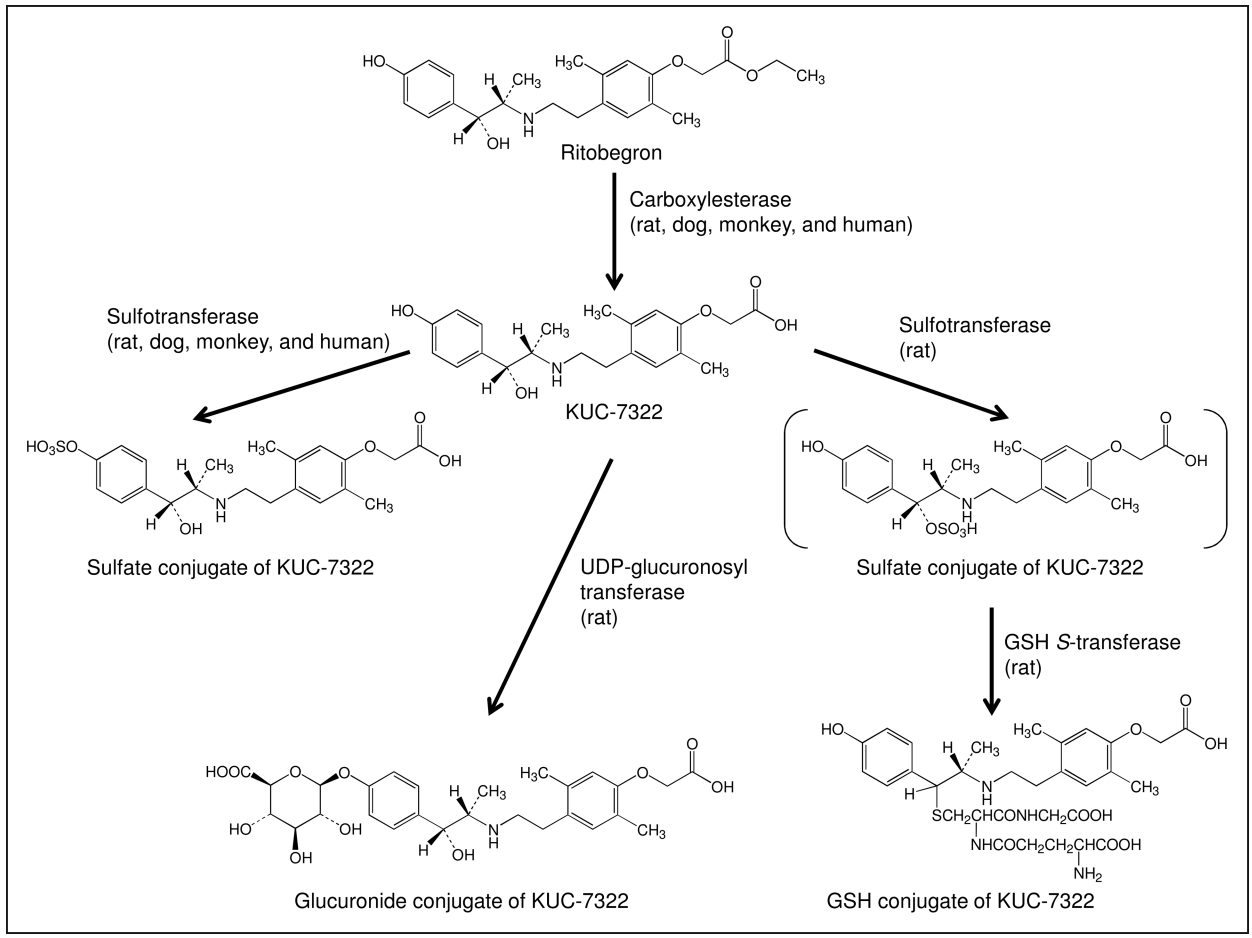

Fig. 4: Proposed metabolic pathway for ritobegron. This pathway was proposed from in vitro metabolism data for ritobegron in liver subcellular fractions.

resulting in the formation of reactive electrophilic carbocation or nitrenium ion intermediates that covalently bind to cellular macromolecules and potentially lead to mutagenicity and carcinogenicity (Glatt 1997; Yi et al. 2006).

GSH *S*-transferase primarily catalyzes the conjugation of reduced GSH to electrophilic compounds and mediates the reduction of organic hydroperoxides, thereby preventing cytotoxicity or mutagenicity. KUC-7322 has a benzylic alcohol structure, and sulfate conjugation of this position was catalyzed sulfotransferases in rat liver S9 fractions. The sulfate conjugate was converted into a reactive electrophilic metabolite, which was assumed to be a benzylic radical, and detoxification of this metabolite by GSH *S*-transferase occurred. The GSH conjugate of KUC-7322 was likely formed by this mechanism in rat liver S9 fractions.

Metabolism is one of the important routes for the clearance of drugs from the body. Inhibition of drug metabolizing enzymes can affect the pharmacokinetics of co-administered drugs. CYP is an important class of phase I enzymes in the biotransformation of drugs. Neither ritobegron nor KUC-7322 inhibited the metabolism of CYP1A2, CYP2A6, CYP2C9, CYP2C19, CYP2D6, CYP2E1, and CYP3A4 probe substrates. Moreover, ritobegron was not metabolized by CYP enzymes. Thus, it was suggested that ritobegron and KUC-7322 have no potential to induce CYP-mediated DDI.

Recently, it has been recognized that membrane transporters can be major determinants of the pharmacokinetic, safety, and efficacy of drugs. Therefore, we assessed the effects of ritobegron and KUC-7322 on P-gp mediated digoxin transport. Digoxin transport was inhibited by ritobegron ($IC_{50} = 58.2\ \mu M$) but not by KUC-7322. As ritobegron is rapidly hydrolyzed in the circulation, the main consideration was the potential for inhibition of the intestinal P-gp-mediated transport. We investigated the inhibitory effects of KUC-7322 on the uptake of probe substrates using S2 cells stably expressing OAT1, OAT2, OAT3, OCT2, OCT3, and OCTN1. KUC-7322 exhibited little or no inhibitory effects on all these transporters.

In addition, we investigated the uptake of KUC-7322 in S2 cells stably expressing OAT3 since the uptake of the probe substrate was slightly inhibited by KUC-7322. Significant uptake of KUC-7322 was observed, indicating that KUC-7322 was a substrate of OAT3.

Five isoforms of OAT family have been identified. OAT1, OAT2, OAT3, and OAT4 are expressed in the human kidney. OAT1, OAT2, and OAT3 are localized on the basolateral membrane and OAT4 is localized in the brush border membrane. Each of these transporters has similar substrate specificity (Sekine et al. 2004; Shitara et al 2005). Clinically relevant OAT-mediated DDI have been seen with probenecid. When combined with probenecid, cidofovir, a substrate of OAT1, showed a 32% decrease in clearance (Cihlar et al. 1999), and furosemide, a substrate of OAT1 and OAT3, showed a 66% decrease in clearance (Hasannejad et al. 2004). These interactions were observed in humans (Li et al. 2006; Cundy 1999). A decrease in clearance and an increase in AUC for KUC-7322 may be seen in combination with probenecid in humans.

In conclusion, there are species differences in the hydrolysis and conjugation of ritobegron. CYP-mediated DDI are not likely to occur when ritobegron is administered in combination with CYP substrates or inhibitors. Furthermore, there may be an increase in the plasma concentrations of substrates of P-glycoprotein, such as digoxin, when administered in combination with ritobegron.

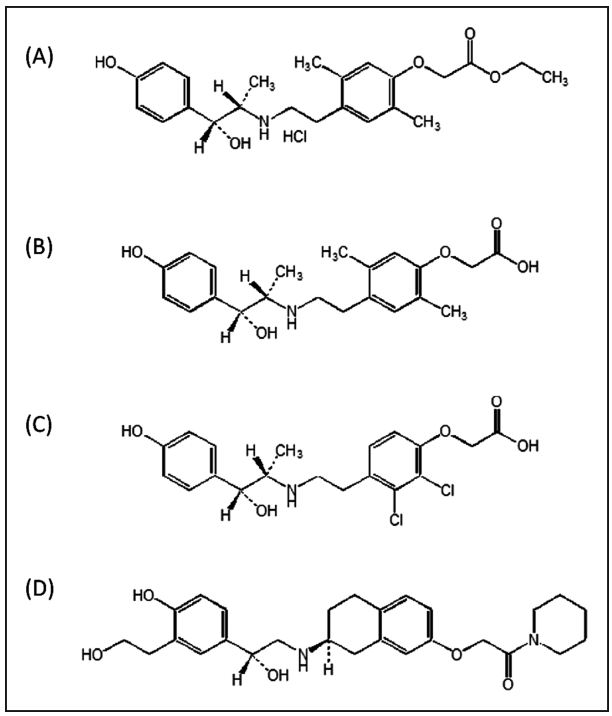

Fig. 5: Chemical structure of ritobegron (A), KUC-7322 (B), UL092 (C), and KUR-1243 (D). *: 14C-labeled position of labeled compound.

In addition, there may be an increase in the plasma concentration of KUC-7322 when administered in combination with OAT inhibitors, such as probenecid.

4. Experimental

4.1. Materials

Ritobegron, KUC-7322, UL092, and KUR-1243 were synthesized by Kissei Pharmaceutical Co. Ltd (Nagano, Japan). Their chemical structures are shown in Fig. 5. [^{14}C]Ritobegron was synthesized by Amersham Pharmacia Biotech UK Ltd. (Buckinghamshire, UK). The specific activity was 2.15 GBq/mmol and radiochemical purity was greater than 95% as determined by high performance liquid chromatography (HPLC). PAH sodium salt, BNPP, chlorzoxazone, coumarin, dextromethorphan, 7-ethoxyresorufin, eserine, estrone sulfate potassium salt, histamine dihydrochloride, 7-hydroxycoumarin (umbelliferone), nifedipine, PMSF, PGF2α tris salt, resorufin sodium salt, tolbutamide, Dulbecco's Modified Eagle's Medium with 4.5 g/L glucose (DMEM), nonessential amino acids, L-glutamine, 0.25% trypsin-EDTA, penicillin-streptomycin, and Hank's balanced salt solution (HBSS) were purchased from Sigma-Aldrich Co. (St Louis, MO, USA). Tetraethylammonium bromide (TEA) was purchased from Wako Pure Chemical industries Ltd. (Osaka, Japan). Dextrorphan, 6-hydroxychlorzoxazone, (±)-4'-hydroxymephenytoin, hydroxytolbutamide, oxidized nifedipine, and *S*-mephenytoin were purchased from Gentest. (Wobum, MA, USA). Fetal bovine serum (FBS) was purchased from Life Technologies (Carlsbad, CA, USA). RITC 80-7 culture medium was purchased from Medical and Biological Laboratories Co. Ltd (Aichi, Japan). [^{14}C]PAH, [^{3}H]Digoxin, [^{3}H] estrone sulfate, ammonium salt, [^{3}H]histamine dihydrochloride, [^{3}H]mannitol, [^{3}H]PGF2α, Ultima Flo-M, scintillation cocktail for HPLC, and Hionic-Fluor, scintillation cocktail, Aquasol-2, scintillation cocktail, were purchased from PerkinElmer Life and Analytical Sciences (Waltham, MA, USA). [^{14}C]Tetraethylammonium bromide (TEA) was purchased from American Radiolabeled Chemicals (St Louis, MO, USA). Pooled liver microsomes from rat (Sprague-Dawley), dog (beagle), monkey (cynomolgus), and human were purchased from XenoTech, LLC (Lenexa, KS, USA) and Tissue Transformation Technologies (Edison, NJ, USA). Pooled liver S9 fractions from rat, dog, and monkey were purchased from Biopredic International (Saint-Gregoire, France) and human pooled liver S9 fractions were purchased Tissue Transformation Technologies. All other chemicals used in this study were of analytical grade and purchased commercially. Transwells (12-well, 11-mm diameter, 0.4 μm pores) were purchased from Corning Costar (Cambridge, MA, USA).

4.2. In vitro species differences in metabolism of ritobegron in liver microsomes

Following pre-incubation at 37 °C for 5 min, pooled liver microsomes (1 mg protein/mL) from rat, dog, monkey, and human were incubated at 37 °C for 120 min with [^{14}C]ritobegron (300 μM) in 100 mM potassium phosphate buffer (pH 7.4) in the presence or absence of an NADPH generating system (consisting of 1 mM β-NADP$^+$, 5 mM glucose 6-phosphate, 3 mM $MgCl_2$, and 1 U/mL glucose 6-phosphate dehydrogenase), at a final incubation volume of 0.2 mL. The reaction was initiated by addition of ritobegron solution. Each experiment was performed in duplicate.

4.3. In vitro species differences in hydrolysis of ritobegron in liver S9 fractions and serum

Following pre-incubation at 37 °C for 5 min, pooled liver S9 fractions or serum from rat, dog, monkey, and human were incubated at 37 °C for 5 min with ritobegron in 50 mM Tris-HCl buffer (pH 7.4, containing 0.154 M KCl), at a final incubation volume of 200 μL. The reaction was initiated by addition of ritobegron solution. Final liver S9 protein concentrations for rat, dog, monkey, and human in the reaction mixture were 0.0520, 0.0491, 0.0483, and 0.025 mg protein/mL, respectively. Final serum concentration for rat, dog, monkey, and human in the reaction mixture were 0.5, 50, 100, and 50 μL/mL reaction mixture, respectively. The final concentration of ritobegron in reaction mixtures was 5, 10, 20, 50, 100, 200, 500, or 1,000 μM. Each experiment was performed in duplicate.

4.4. In vitro species differences in formation of KUC-7322 conjugate metabolites

For formation of glucuronide conjugates of KUC-7322, pooled rat and human liver microsomes (1 mg protein/mL) were incubated at 37 °C for 120 min with 50 μM [^{14}C]KUC-7322 in 100 mM Tris-HCl buffer (pH 7.4) containing 5 mM $MgCl_2$, 0.5 mg/mg Brij 58, and 3 mM uridine 5'-diphosphoglucuronic acid (UDPGA), at a final incubation volume of 200 μL. Each experiment was performed in duplicate.

For formation of sulfate conjugates of KUC-7322, pooled rat and human liver S9 fractions (3 mg protein/mL) were incubated at 37 °C for 120 min with 50 μM [^{14}C]KUC-7322 in 100 mM phosphate buffer (pH 7.4) containing 5 mM $MgCl_2$, and 1 mM PAPS at a final incubation volume of 200 μL. Each experiment was performed in duplicate.

For formation of glutathione conjugates of KUC-7322, pooled rat and human liver S9 fractions (3 mg protein/mL) were incubated at 37 °C for 120 min with 50 μM [^{14}C]KUC-7322 in 100 mM phosphate buffer (pH 7.4) containing 5 mM GSH and one of the following: 1) 5 mM $MgCl_2$, 2) NADPH re-generating system (consisting of 1 mM β-NADP$^+$, 5 mM glucose 6-phosphate, 3 mM $MgCl_2$, and 1 U/mL glucose 6-phosphate dehydrogenase), 3) 3 mM UDPGA and 5 mM $MgCl_2$, and 4) 1 mM PAPS and 5 mM $MgCl_2$ at a final incubation volume of 200 μL. Each experiment was performed in duplicate.

4.5. Effects of esterase inhibitors on hydrolysis of ritobegron

Following pre-incubation with PMSF, a serine protease inhibitor, eserine, a choline esterase inhibitor, and BNPP, a carboxylesterase inhibitor, at 37 °C for 10 min, human liver microsomes were incubated at 37 °C for 5 min with ritobegron (50 μM) in 100 mM phosphate buffer (pH 7.4), at a final incubation volume of 0.4 mL. The reaction was initiated by addition of ritobegron solution. Final concentrations of PMSF, eserine, and BNPP were 10, 100, and 1,000 μM. Each experiment was performed in duplicate.

4.6. Metabolite analysis by radio-HPLC

All incubations were terminated by addition of 200 μL of ice-cold acetonitrile. The solution was centrifuged (15,900 × *g*, 2 min, room temperature), and the supernatant was evaporated to dryness at room temperature under a nitrogen stream. The residue was reconstituted in 200 μL of 10 mM ammonium acetate/methanol (80:20, v/v). After centrifugation (15,900 × *g*, 2 min, room temperature), the supernatant (20 μL) was injected into the HPLC system (HP1100, Agilent Technologies, Santa Clara, CA, USA). Separation of KUC-7322 and its metabolites was achieved using a reverse phase analytical column, Mightysil RP-18 GP (3 μm, 150 mm × 3.0 mm i.d., Kanto Kagaku, Tokyo, Japan). The mobile phase was mixture of 10 mM ammonium acetate (A) and methanol (B). The mobile phase was passed over the column at 0.5 mL/min in the following linear gradient: starting with 20% B, increasing to 30% B from 0 to 10 min, increasing to 100% B from 10 to 20 min, maintaining 100% B from 20 to 25 min, decreasing to 20% B from 25 to 25.1 min, and finally maintaining 20% B from 25.1 to 35 min. The column was maintained at 30 °C. The column eluate was added to a flow scintillation analyzer (FSA, Radiomatic 525TR, PerkinElmer Life and Analytical Sciences). The elution pattern of metabolites was determined using

the FSA with 6 s integration. Ultima Flo-M (PerkinElmer Life and Analytical Sciences) was added to HPLC eluate at a flow rate three times that of the mobile phase. Peak integration of the UV and radioactivity were performed using FLO-ONE for Windows Analysis, version 3.6.0, (PerkinElmer Life and Analytical Sciences).

4.7. Quantification of KUC-7322 using HPLC

All incubations were terminated by addition of 200 or 300 μL of ice-cold acetonitrile. UL092 or KUR-1243 (internal standards, 100 μg/mL, 100 μL) was added to the reaction mixture and the solution was centrifuged (20,800 × *g*, 2 min) after mixing thoroughly. The supernatant was dried under a stream of nitrogen gas at 40 °C. The residue was dissolved in 20 mM potassium phosphate (pH 3.0)/acetonitrile (8:2, v/v) (200 μL), and a sample of the product (50 μL) was injected into the HPLC system (L-7000, Hitachi, Ibaraki, Japan). Separation of KUC-7322 and its internal standard was achieved with a Luna C8 (2) (5 μm, 150 mm × 4.6 mm i.d., Phenomenex, Torrance, CA, USA). The mobile phase was a mixture of 20 mM potassium phosphate (pH 3.0) (A) and 20 mM potassium phosphate (pH 3.0)/acetonitrile (50:50, v/v) (B). The mobile phase was passed through the column at 1 mL/min in the following linear gradient: starting with 30% B, increasing to 70% B from 0 to 15 min, maintaining 70% B from 15 to 17 min, increasing 100% B from 17 to 18 min, maintaining 100% B from 18 to 23 min, decreasing to 30% B from 23 to 24 min, and finally maintaining 30% B from 24 to 34 min. The column was maintained at 40 °C. KUC-7322 was detected with a fluorescence detector (L-7480, Hitachi) with an excitation wavelength of 225 nm and a detection wavelength of 302 nm. The D-7000 HPLC System Manager, version 3.1.1, (Hitachi) was used to determine the plasma concentrations of KUC-7322.

4.8. Calculation of kinetic parameters

The concentration of KUC-7322 formed during incubation was determined as formation velocity (nmol/min/mg protein) by the equation below, and plotted on an Eadie-Hofstee plot. The slope and intercept of Eadie-Hofstee plot were determined by least squares regression, and from these values, the K_m and V_{max} for KUC-7322 formation were calculated.

If the Eadie-Hofstee plot for KUC-7322 formation was nonlinear, [V (velocity): KUC-7322 formation velocity] versus [S (substrate concentration); ritobegron concentration] curves were fit by nonlinear least squares regression to a two-enzyme Michaelis-Menten model using extrapolated data from the Eadie-Hofstee plot as initial parameters. The K_m and V_{max} were determined using WinNonlin Professional version 3.1 (Pharsight, Mountain View, CA, USA). The equation for KUC-7322 formation velocity using a two-enzyme Michaelis-Menten model were shown below.

Equation for KUC-7322 formation velocity:

$$\text{KUC} - 7322\ \text{formation velocity (nmol/ min /mL)} = \frac{\text{KUC} - 7322\ \text{concentration formed by incubation } (\mu\text{M})}{\text{Serum content in mixture } (\mu\text{L/mL}) \times \text{reaction time (5 min)}}$$

Two-enzyme Michaelis-Menten model:

$$\text{KUC} - 7322\ \text{formation velocity (nmol/ min /mL)} \quad \frac{V_{max\,1} \times [S]}{K_{m1} + [S]} + \frac{V_{max\,2} \times [S]}{K_{m2} + [S]}$$

[S]: ritobegron concentration

4.9. CYP inhibition assay

The inhibition of CYP enzymes (CYP 1A2, 2A6, 2C9, 2C19, 2D6, 2E1, and 3A4) by ritobegron and KUC-7322 was assessed in human liver microsomes using LC-MS/MS as previously described (Yin 2000). Briefly, the reaction mixture contained a final concentration of 0.1 M potassium phosphate buffer (pH 7.4), 5 mM $MgCl_2$, 0.1 mM EDTA, 1 mM NADPH, human liver microsomes, and the CYP substrate in a total volume of 0.2 mL. The reaction mixture without NADPH was pre-incubated at 37 °C for 5 min. NADPH was added to initiate the reaction. Following incubation for 20 min at 37 °C, the reaction was stopped by solid-phase extraction (SPE) using an OASIS HLB (1 cc, 10 mg, Waters, Milford, MA, USA) column. The SPE column was equilibrated with 0.5 mL of methanol and 0.5 mL of distilled water. The entire reaction mixture was applied to the SPE column. The reaction mixtures of the seven CYP substrates were applied to the same SPE column serially. The column was then washed with 1 mL of distilled water. The water was eliminated by aspiration, and elution was performed with 0.2 mL of methanol. Phenacetin (100 μL, 2 μM) was added as an internal standard. Quantification of the metabolites of the CYP substrates was carried out on a HPLC system (HP1100, Agilent Technologies) coupled to a tandem mass spectrometer (TSQ7000, Thermo Quest, San Jose, CA, USA) with an electrospray ionization source in selected reaction monitoring mode. Separation of the metabolites of the CYP substrates was achieved with a Luna C8 (2) (5 μm, 150 mm × 2.0 mm i.d., Phenomenex). The mobile phase was a 0.1% (v/v) acetic acid (A) and methanol (B). The mobile phase was pumped through the column at 0.2 mL/min in the following linear gradient: starting with 46% B, increasing to 100% B from 0 to 2.5 min, and finally decreasing 46% B from 2.5 to 2.6 min. The column was maintained at 30 °C. A 25 μL sample of the reaction mixture was injected into the column. The amount of metabolite formed for each CYP substrate was determined using data analysis software (Xcalibur LC Quan Ver. 1.0, Thermo Quest). The determinations were based on a calibration curve for each metabolite constructed from the peak area ratio (Y) of metabolites and the internal standard, and the metabolite concentration (X; 25, 50, 100, 250, 1000, 2500, and 5000 nM). The calibration curve was prepared with $1/X^2$ weighting.

4.10. OATs, OCTs, and OCTN uptake/inhibition assay

OATs, OCTs, and OCTN uptake/inhibition assays were completed at Fuji Biomedix Co. Ltd. (Yamanashi, Japan). OAT1-, OAT2-, OAT3-, OCT2-, OCT3-, and OCTN1-expressing S2 cells and vector (pcDNA3.1)-expressing S2 cells (mock-transfected cells) were cultured in RITC 80-7 culture medium (1 L) supplemented with 3.3 g of HEPES, 10 mg of transferrin, 80 units of insulin, 10 μg of epidermal growth factor, 400 mg of Geneticin® sulfate, and 5% FBS (pH 7.2) at 33 °C in humidified atmosphere with 5% CO_2 (Takeda et al 2002). The parental S2 cell line was derived from the S2 portion of the renal proximal tubules and carries a temperature-sensitive simian virus 40 large T-antigen gene. Transporter or vector-expressing S2 cells were seeded at a density of 1×10^5 to 5×10^5 cells/well in 24-well tissue culture plates (Corning Costar) individually expressing either OAT1, OAT2, OAT3, OCT2, OCT3, or OCTN1 and cultured for 2 days. These cells were used at passage numbers 15 to 23.

For inhibition studies, KUC-7322, and positive control inhibitors (probenecid, benzbromarone, probenecid, imipramine, and quinidine for OAT1, OAT2, OAT3, OCTs, and OCTN1, respectively) were added at a final concentration of 30 μM into uptake medium (Dulbecco's phosphate-buffered saline (DPBS), pH 7.4) containing the radiolabeled substrates. Following pre-incubation for 10 min, cells were incubated for 2 min for OAT1 and OAT3 cells, 0.5 min for OAT2 cells, 5 min for OCT2 and OCTN1 cells, or 1 min for OCT3 cells.

For uptake studies, [^{14}C]KUC-7322 was added at final concentrations of 5, 50, 100, 150, 200, 250, and 300 μM to the uptake medium (DPBS, pH 7.4). OAT3-expressing cells were incubated for 0.5, 1, 2, 5, 15, or 30 min. After incubation, the solution was removed and uptake was stopped by adding ice-cold DPBS, followed by washing twice with the same solution. Cells were lysed with 0.5 mL of 0.1 M sodium hydroxide and the lysate collected from the wells. Following addition of 3 mL of Aquasol-2 to the lysate, radioactivity was determined by LSC (Tri-Carb 3100TR, PerkinElmer Life and Analytical Sciences). Protein concentrations in the cell lysates were determined using the BCA Protein Assay Reagent (Pierce, Rockford, IL, USA).

4.11. P-gp Inhibition assay

Caco-2 cells (American Type Cell Collection, Manassas, VA, USA) were grown in a manner similar to that reported previously (Shirasaka et al. 2006; Siissalo et al 2007). Briefly, Caco-2 cells were cultured in DMEM supplemented with 1% L-glutamine, 1% non-essential amino acids, 100 U/mL penicillin, 100 μg/mL streptomycin, 10 nM vinblastine and 10% FBS at 37 °C in 75-cm^2 culture flasks (Corning Costar) in humidified atmosphere with 5% CO_2. Confluent cells were sub-cultured every 7 days by treatment with 0.25% trypsin-EDTA. Caco-2 cells were seeded at a density of 6.3×10^4 cells/well on polycarbonate filters inside Transwells. The culture medium (0.5 mL in the apical side and 1.5 mL in the basolateral side) was changed three times a week. Cells were cultured on filters for 21 days to form differentiated confluent monolayers. Cells of passage numbers 29 and 30 were used in the P-gp assay.

The Caco-2 cell monolayers were washed with pre-warmed HBSS (pH 7.4) at 37 °C twice. Then, the transepithelial electrical resistance was measured using a transepithelial resistance measurement device (Millicell-ERS, Millipore, Billerica, MA, USA). After that, Caco-2 cell monolayers were incubated in pre-incubation buffer (HBSS containing ritobegron, KUC-7322, or verapamil) for 30 min. The donor chamber solution (apical or basolateral side) was replaced with transport buffer (pre-incubation buffer containing 1 μM [^{3}H]digoxin or 1 μM [^{3}H]mannitol), and incubated at 37 °C in a CO_2 incubator. After incubation for 30 min, 100 μL of the solution was collected from the receiver chamber. Following addition of 3 mL of Hionic-Fluor, radioactivity was measured using LSC (Tri-Carb 3100TR, PerkinElmer Life and Analytical Sciences) to determine the concentration

of [^{3}H]digoxin or [^{3}H]mannitol in the solution. The permeation coefficient (P_{app}) value was calculated using the following equation:

$$P_{app} = \frac{V_R}{A \times C_0} \times \frac{dC}{dt}$$

V_R is the volume in the receiver chamber (mL), A is the filter surface area (1.13 cm^2), C_0 is the initial concentration (μM), and dC/dt is the permeation velocity (nM/s). The P_{app} was used to calculate the efflux ratio (ER = P_{app} basolateral to apical/P_{app} apical to basolateral).

References

Abe Y, Ota E, Endo T, Murakami M, Kobayashi M (2014) Absorption, disposition, metabolism, and excretion of ritobegron (KUC-7483), a novel selective β3-adrenoceptor agonist, in rats. Pharmazie: doi: 10.1691/ph.2014.4679.

Aldridge WN (1993) The esterases: perspectives and problems. Chem Biol Interact 87: 3–13.

Cihlar T, Lin DC, Pritchard JB, Fuller MD, Mendel DB, Sweet DH (1999) The antiviral nucleotide analogs cidofovir and adefovir are novel substrates for human and rat renal organic anion transporter 1. Mol Pharmacol 56: 570–508.

Cundy KC (1999) Clinical pharmacokinetics of the antiviral nucleotide analogues cidofovir and adefovir. Clin Pharmacokinet 36: 127–143.

Glatt H (1997) Sulfation and sulfotransferases 4: Bioactivation of mutagens via sulfation. FASEB J 11: 314–321.

Hasannejad H, Takeda M, Taki K, Shin HJ, Babu E, Jutabha P, Khamdang S, Aleboyeh M, Onozato ML, Tojo A, Enomoto A, Anzai N, Narikawa S, Huang XL, Niwa T, Endou H (2004) Interaction of human organic anion transporters with diuretics. J Pharmacol Exp Ther 308: 1021–1029.

Hosowaka M, Furihata T, Yaginuma Y, Yamamoto N, Koyano N, Fujii A, Nagahara Y, Satoh T, Chiba K (2007) Genomic structure and transcriptional regulation of the rat, mouse, and human carboxylesterase genes. Drug Metab Rev 39: 1–15.

Humerickhouse R, Lohrbach K, Li L, Bosron WF, Dolan E (2000) Characterization of CPT-11 hydrolysis by human liver carboxylesterase isoforms hCES-1 and hCES-2. Cancer Res 60: 1189–1192.

Igawa Y, Schneider T, Yamazaki Y, Tatemichi S, Homma Y, Nishizawa O, Michel MC (2012) Functional investigation of β-adrenoceptors in human isolated detrusor focusing on the novel selective β3-adrenoceptor agonist KUC-7322. Naunyn Schmiedebergs Arch Pharmacol 385: 759–767.

Imai T, Taketani M, Shii M, Hosokawa M, Chiba K (2006) Substrate specificity of carboxylesterase isozymes and their contribution to hydrolase activity in human liver and small intestine. Drug Metab Dispos 34: 1734–1741.

James GT (1978) Inactivation of the protease inhibitor phenylmethylsulfonyl fluoride in buffer. Anal Biochem 86: 574–579.

Kraut D, Goff H, Pai RK, Hosea NA, Silman I, Sussman JL, Taylor P, Voet JG (2000) Inactivation studies of acetylcholinesterase with phenylmethylsulfonyl fluoride. Mol Pharmacol 57: 1243–1248.

Li B, Sedlacek M, Manoharan I, Boopathy R, Duysen EG, Masson P, Lockridge O (2005) Butyrylcholinesterase, paraoxonase, and albumin esterase, but not carboxylesterase, are present in human plasma. Biochem Pharmacol 70: 1673–1684.

Li M, Anderson GD, Wang J (2006) Drug-drug interactions involving membrane transporters in the human kidney. Expert Opin Drug Metab Toxicol 2: 505–532.

Maruyama I, Goi Y, Tatemichi S, Maruyama K, Hoyano Y, Yamazaki Y, Kusama H (2012a) Bladder selectivity of the novel β3-agonist ritobegron (KUC-7483) explored by in vitro and in vivo studies in the rat. Naunyn Schmiedebergs Arch Pharmacol 385: 845–852.

Maruyama I, Tatemichi S, Goi Y, Maruyama K, Hoyano Y, Yamazaki Y, Kusama H (2012b) Effect of ritobegron (KUC-7483), novel selective β3-adrenoceptor agonist, on bladder function in cynomolgus monkey. J Pharmacol Exp Ther 342: 163–168.

Morton CL, Wadkins RM, Danks MK, Potter PM (1999) The anticancer prodrug CPT-11 is a potent inhibitor of acetylcholinesterase but is rapidly catalyzed to SN-38 by butyrylcholineesterase. Cancer Res 59: 1458–1463.

Satoh T, Taylor P, Bosron WF, Sanghani SP, Hosokawa M, La Du BN (2002) Current progress on esterases: From molecular structure to function. Drug Metab Dispos 30: 488–493.

Sekine T, Miyazaki H, Endou H (2004) Molecular physiology of renal organic anion transporters. Am J Physiol Renal Physiol 290: F251-F261.

Shirasaka Y, Kawasaki M, Sakane T, Omatsu H, Moriya Y, Nakamura T, Sakaeda T, Okumura K, Langguth P, Yamashita S (2006) Induction of human P-glycoprotein in Caco-2 cells: Development of a highly sensitive assay system for P-glycoprotein-mediated drug transport. Drug Metab Pharmacokinet 21: 414–423.

Shitara Y, Sato H, Sugiyama Y (2005) Evaluation of drug-drug interaction in the hepatobiliary and renal transport of drug. Annu Rev Pharmacol Toxicol 45: 689–723.

Siissalo S, Laitinen L, Koljonen M, Vellonen K, Kortejärvi H, Urtti A, Hirvonen J, Kaukonen AM (2007) Effect of cell differentiation and passage number on the expression of efflux proteins in wild type and vinblastine-induced Caco-2 cell lines. Eur J Pharm Biopharm 67: 548–554.

Simeon V, Reiner E, Škrinjaric-Špoljar M (1988) Cholinesterases in rabbit serum. Gen Pharmacol 19: 849–853.

Takeda M, Khamdang S, Narikawa S, Kimura H, Kobayashi Y, Yamamoto T, Cha S H, Sekine T Endou H (2002) Human organic anion transporters and human organic cation transporters mediate renal antiviral transport. J Pharmacol Exp Ther 300: 918–924.

White KN, Eggermont J, Hope DB (1987) Effect of the carboxylesterase inhibitor bis-(4-nitrophenyl)phosphate *in vivo* on aspirin hydrolase and carboxylesterase activities at first-pass sites of metabolism in the guinea pig. Biochem Pharmacol 36: 2687–2688.

Williams FM (1985) Clinical significance of esterases in man. Clin Pharnacokinet 10: 392–403.

Xu G, Zhang W, Ma MK, McLeod HL (2002) Human carboxylesterase 2 is commonly expressed tissue and is correlated with activation of irinotecan. Clin Cancer Res 8: 2605–2611.

Yi L, Dratter J, Wang C, Tunge JA, Desaire H (2006) Identification of sulfation sites of metabolites and prediction of the compounds' biological effects. Anal Bioanal Chem 386: 666–674.

Yin H, Racha J, Li SH, Olejnik N, Satoh H, Moore D (2000) Automated high throughput human CYP isoform activity using SPE-LC/MS method: application in CYP inhibition evaluation. Xenobiotica 30: 141–154.